A computer model for a high temperature fuel cell

E. Hernández-Pacheco
Systems Research Center-Mexico,
Intel, Tlaquepaque, Jalisco,
Tel. Office:+52 3335406024, Fax:+52 3335406099,
e-mail: eduardo.hernandez.pacheco@intel.com

M.D. Mann
Department of Chemical Engineering,
University of North Dakota, Grand Forks-ND,
e-mail: mikemann@mail.und.nodak.edu

Recibido el 30 de marzo de 2005; aceptado el 16 de febrero de 2006

A computer model is developed for determining the performance characteristics (*e.g.*, current-voltage curves) of a solid oxide fuel cell. The model determines the fuel/oxidant concentration, the temperature profiles and the current density along the fuel and oxidant channels, respectively. Then, the average of the local current density distribution is used to determine the current-voltage curves (IV curves) over the entire range of cell potential, *i.e.*, from open circuit voltage to short circuit voltage.

Keywords: Fuel cells; electrochemistry; computer modeling.

Se desarrolla un modelo por computadora para determinar las características de desempeño (*e.g.*, curvas de corriente y voltaje) de una celda de combustible de óxido sólido. El modelo determina la concentración de combustible/oxidante, el perfil de temperaturas y la densidad local de corriente a lo largo de los canales de combustible y oxidante, respectivamente. Posteriormente, el promedio de la distribución de la densidad de corriente se usa para crear las curvas de corriente-volataje en el intervalo completo del potencial de la celda, *i.e.*, desde el voltaje de circuito abierto hasta el voltage de corto circuito.

Descriptores: Celdas de combustible; electroquímica; modelo computacional.

PACS: 82.47.Ed; 82.47.-a; 07.05.Tp

1. Introduction

Fuel cells are electrochemical devices capable of converting chemical energy into electricity by reversing the electrolysis dissociation of water. Thus the byproducts of a fuel cell reaction are water and depleted fuel (hydrogen and oxygen). Therefore fuel cells are regarded as a pollution-free technology. The following equations are assumed to be relevant if a fuel cell is operated with hydrogen and air as fuel and oxidant, respectively [1]:

$$\text{Anode}: \quad \mathrm{H_2} + \mathrm{O^{=}} \rightarrow \mathrm{H_2O} + 2\,e^{-} \tag{1}$$

$$\text{Cathode}: \quad \tfrac{1}{2}\mathrm{O_2} + 2\,e^{-} \rightarrow \mathrm{O^{=}} \tag{2}$$

$$\text{Cell}: \quad \mathrm{H_2} + \tfrac{1}{2}\mathrm{O_2} \rightarrow \mathrm{H_2O} \tag{3}$$

In the former equations, the electrolyte is assumed to carry oxygen ions from the cathode side to the anode side; thus water is produced in the anode side of the cell.

Fuel cells can be used in a wide range of applications according to their operating temperature and type of electrolyte. For example, low temperature fuel cells can be used in portable devices or fuel cell cars, while high temperature fuel cells can be used for stationary power generation. In addition, some applications (*e.g.*, spacecraft industry) require a solid electrolyte so that the cell can be configured in different positions without risk of leakage or uneven distribution of the electrolyte material. The most developed type of fuel cells are the polymeric electrolyte membrane (PEM) fuel cells. This low temperature fuel cell uses a polymeric membrane that conducts protons from the anode to the cathode at relative low temperatures ($\approx 80^{\circ}$C) as long as the membrane is well hydrated [2]. The low operating temperature and the solid membrane make PEMs ideal for portable applications such as breathalyzers, cell phones, laptops, etc. Moreover, the low operating temperature will allow fast start ups if used in fuel cell cars. The most developed high temperature fuel cells are the solid electrolyte fuel cells (SOFCs). SOFCs use a ceramic electrolyte (Yttria-stabilized zirconia) that exhibits high ionic conductivities at elevated temperatures (≈ 1073 K) [3]. The high operating temperature constrains SOFCs to stationary applications, but allows the use of a variety of fuels such as natural gas and carbon monoxide, unlike PEM fuel cells that poison with ppm levels of carbon monoxide. The flexibility of the fuel choice gives SOFCs the advantage of cogeneration and bottoming cycles. In either case, low or high temperature, fuel cells are attracting a lot of attention as an alternative clean-energy technology, in part to the predictions of oil shortages in a few decades and the increasing evidence of global warming due to greenhouse gases.

In this document, we present a simple, but useful, computer model for predicting the performance characteristics (IV curves) of a solid oxide fuel cell. This simplified model is based on a more detailed work previously published by the authors [4]. In summary, this model uses a more accurate

description of the activation and concentration polarization instead of semi-empirical correlations [5]. An extensive literature review of previous modeling-efforts and the advantages of this work can be found at [4]. Figure 1 shows a typical configuration for a planar design of a solid oxide fuel cell. The bipolar plate shown in the figure serves as a structure for the distribution of fuel and oxidant to the cell and also as current collectors (interconnects). The figure also shows the principal modes of flow distribution. In this paper the co-flow configuration is chosen for the sake of simplicity. Accordingly, we present a 1-D, steady state, single-phase, non-isothermal model for a co-flow configuration using pure hydrogen and air as fuel and oxidant.

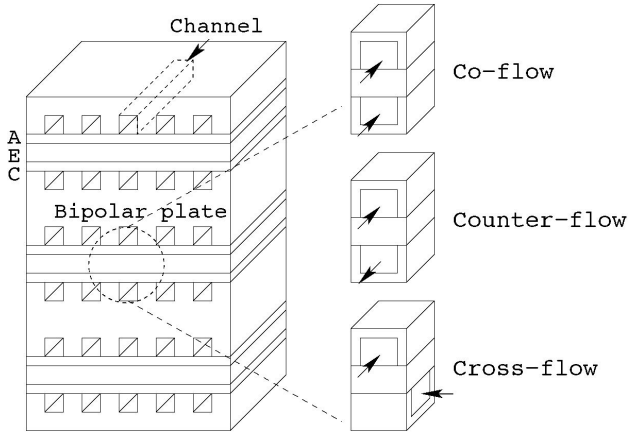

FIGURE 1. Planar design of a fuel cell stack showing the principal modes of flow distribution: co-flow, counter-flow and cross-flow. The diagram also shows the bipolar plate, the electrodes (A: anode, C: cathode) and the electrolyte (E) of a typical fuel cell stack.

2. Description of the model

The modeling of SOFCs, and fuel cells in general, involves the integration of the electrochemical reactions with the conservation of mass and energy. An electrochemical model will be presented first, and the integration with the conservation equations will be presented later in the paper. However, the system of equations (electrochemical, mass and energy) must be solved simultaneously because the fuel/oxidant consumption and the energy distribution of the cell are related by the local current density. The simplifications of this model are based on the following assumptions. Because SOFCs operate at high temperatures the water produced in the system is always at gas phase (single-phase model). In addition, the model assumes that the fuel and oxidant are uniformly distributed through each channel in the cell; thus the results for one channel are extended to the other channels. The reactions take place only at the electrode-eletrolyte interface, assuming pure electronic conductors as electrodes.

2.1. Electrochemical model

Any energy-conversion system experiences irreversible losses, according to the second law of thermodynamics. In the case of a fuel cell system, these irreversible losses, also know as polarizations, are: activation ($\eta_{\mathcal{A}}$), ohmic ($\eta_{\mathcal{O}}$) and transport losses ($\eta_{\mathcal{D}}$). Therefore, the cell potential is determined by ideal cell potential minus the polarization terms,

$$E = E_o - \eta_{\mathcal{O}} - \eta_{\mathcal{A}} - \eta_{\mathcal{D}}, \tag{4}$$

where E_o indicates the maximum thermodynamic potential, and can be determined by the Nernst equation

$$E_o = \Delta G + \frac{RT}{2\mathcal{F}} \ln\left(\frac{P_{\mathrm{H_2O}}}{P_{\mathrm{H_2}}\, P_{\mathrm{O_2}}^{1/2}}\right), \tag{5}$$

where ΔG indicates the Gibbs free energy, R is the ideal gas constant, T the temperature, and P_i is the partial pressure of species i. Assuming a reversible reaction, the Gibbs free energy is determined from the enthalpy and entropy of the reactions.

Activation loss refers to the activation energy that needs to be overcome in order for the electrochemical reactions to proceed. Activation polarization can be determined by the Butler-volmer equation [5]

$$\frac{j}{j_o} = \exp\left(\frac{\alpha\,\eta_{\mathcal{A}}\,z\,\mathcal{F}}{RT}\right) - \exp\left(\frac{(\alpha-1)\eta_{\mathcal{A}}\,z\,\mathcal{F}}{RT}\right) \tag{6}$$

where j is the local current density, j_o is the exchange current density, α is the electron transfer coefficient, z is the electron transfer per reaction, and $\mathcal{F}$ is Faraday's constant. The exchange current density (j_o) is a measure of the electrocatalytic activity of the electrodes. This model considers the activation polarization at both electrodes where the exchange current density for each electrode is determined by the correlations provided by [6].

Ohmic polarization refers to the electronic and ionic resistance through the electrodes, electrolyte and interconnects. Ohmic polarization is determined by Ohm's law

$$\eta_{\mathcal{O}} = \sum_i j\,\ell_i\,\rho_i, \tag{7}$$

where ℓ_i is the thickness of the component i (anode, cathode, electrolyte) and ρ_i is the resistivity of component i.

Finally, transport losses are associated with the resistance to the flow through the porous electrodes. For the case of SOFCs with thick electrodes ($\approx 200\mu$m), this polarization becomes the rate limiting factor at high current densities and low fuel/oxidant concentrations. The transport or diffusion polarization is given by

$$\eta_{\mathcal{D}} = -\frac{RT}{2\mathcal{F}} \ln\left(\frac{y_{\mathrm{H_2}}\, y_{\mathrm{H_2O,In}}}{y_{\mathrm{H_2O}}\, y_{\mathrm{H_2,In}}}\right), \tag{8}$$

where y_i indicates the concentration of species i in the electrode-electrolyte interface and $y_{i,\mathrm{In}}$ indicates the concentration of species i at inlet conditions. The electrode-electrolyte concentration can be calculated from the diffusion of the gases through a porous medium using Fick's model, the dusty gas model, or the Stefan-Maxwell model. The dusty gas model has been shown to produce more accurate results for SOFCS [7.8].

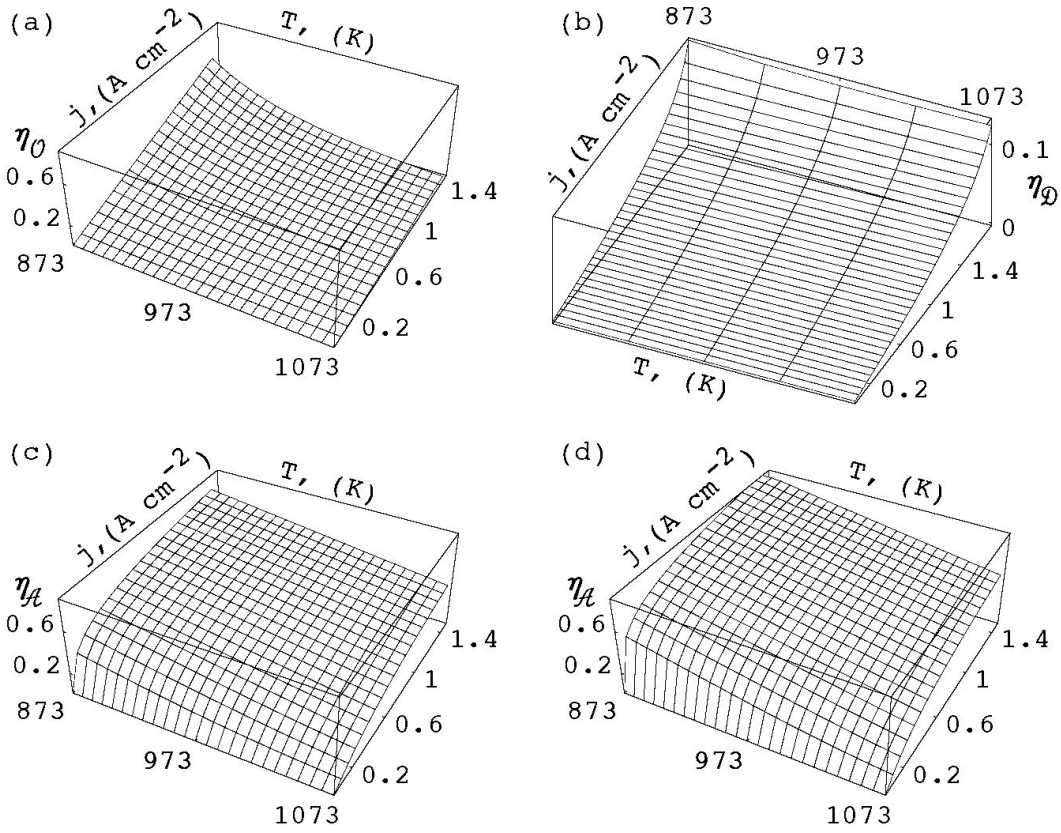

FIGURE 2. Polarization distribution as a funcition of temperature and current density for hydrogen and air as fuel and oxidant, respectively. (a) Ohmic polarization, (b) Transport polarization, (c) Anode activation polarization, and (d) Cathode activation polarization.

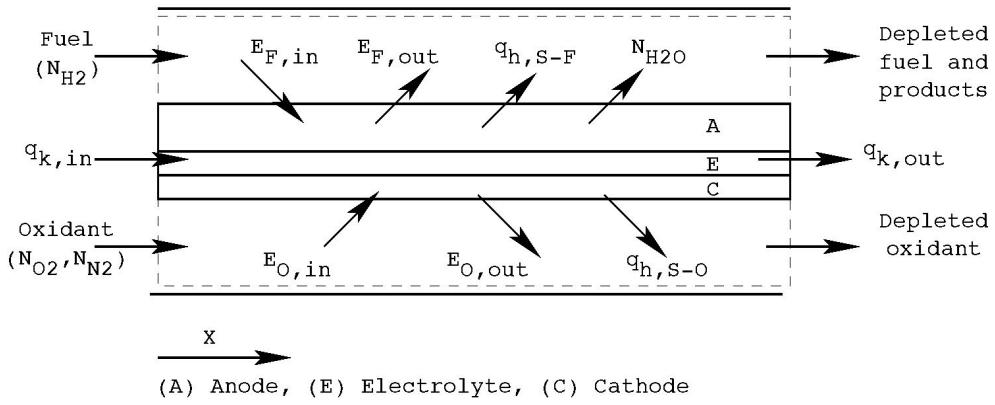

FIGURE 3. The diagram shows a segment of the fuel cell channel modeled. $E_{F,O,in,out}$ indicates the energy due to the mass flow of reaction products and reactants in and out of the fuel cell; $q_{h,s-f,s-a}$ indicates the convective flux of the solid to the fuel/oxidant gas; q_k indicates the heat due to conduction through the solid material; and N_i indicates the molar flux rate of species i.

In Fig. 2, sensitivity to temperature and current density is shown for the three principal modes of polarization; the parameters used in Fig. 2 are representative of a cell operating at 80% of fuel utilization with a thick anode (*i.e.* electrode-supported cell) [5]. Ohmic polarization, Fig. 2a, increases very quickly as the temperature decreases and the current density increases. The thickness of the electrolyte and the temperature will play an important role in the contribution of this polarization as we shall show later. Concentration polarization, Fig. 2b, increases very quickly as the current density increases. At high current density, starvation of fuel becomes more significant and therefore the fuel flow towards the reaction sites is reduced. Activation polarization, Fig. 2c-d, decreases quickly as the temperature increases, and increases with the current density. For SOFCs, activation polarization is more significant during the start-up process and less sig-

nificant once the heat from the electrochemical reactions is released into the system, and therefore the temperature rises.

A careful selection of the design of the cell and the operating conditions can reduce the amount of irreversible losses. For instance, by reducing the thickness of the electrolyte, the ohmic resistance will be lower and the cell can be efficiently operated at lower temperatures [9,10]. However, the use of a thinner electrolyte requires thicker electrodes as support (electrode-supported cell). Electrode-supported cells can operate at lower temperatures (≈ 973 K), reducing the thermal stress induced in the components of the cell; however diffusion limitations will arise at high fuel utilization. Fuel utilization indicates the ratio between the fuel consumed and fuel input to the system; a high fuel utilization translates into an economically efficient operation, and it is a desirable characteristic for fuel cell systems.

2.2. Conservation equations

This model comprises two channels, parallel to each other, divided by the anode-electrolyte-cathode system. A diagram of the energy and mass balances is shown in Fig. 3. The fuel channel contains a mixture of 90% hydrogen ($N_{\mathrm{H_2}}$) and 10% water. While hydrogen flows through the channel, it also diffuses into the porous anode and reacts with oxygen ions coming from the cathode side [see oxidation reaction Eq.(1)]. This reaction releases electrons and produces water ($N_{\mathrm{H_2O}}$). The electrons travel through an external circuit to power an electrical device and reach the cathode side. In the cathode channel, the oxidant (*e.g.* oxygen, $N_{\mathrm{O_2}}$) flows along the channel and diffuses to the cathode-electrolyte interface, where oxygen reacts with the electrons released in the anode to produce oxygen ions [see reduction reaction Eq.(2)]. The oxygen ions then migrate to the anode side through the electrolyte material. The overall process translates into a change in the number of moles of reactants/products and a change in the distribution of energy along the channel.

The mass balance in the fuel and oxidant channels is determined by the fluxes of hydrogen, oxygen and water entering or leaving the electrodes according to

$$\frac{dN_{\mathrm{H_2,O_2,H_2O}}}{dx} = n_{\mathrm{H_2,O_2,H_2O}} \frac{1}{z_{f,a}}, \tag{9}$$

where N_i is the molar flux rate, $z_{f,a}$ is the height of the fuel and air channels, and n_i indicates the flux of species i according to: $-n_{\mathrm{H_2}} = -2\, n_{\mathrm{O_2}} = n_{\mathrm{H_2O}} = j/2\mathcal{F}$.

The energy balance in the channels and the solid are shown next. Here, the solid includes the electrodes, electrolyte and the bipolar plate and it is assumed to be a quasi-homogeneous material with respect to thermal conductivity [11].

Energy balance in the fuel channel:

$$z_f \frac{d\left(N c_p T\right)_f}{dx} = h_f \left(T_s - T_f\right) + c_{p,\mathrm{H_2O}} n_{\mathrm{H_2O}} T_s + c_{p,\mathrm{H_2}} n_{\mathrm{H_2}}\, T_f, \tag{10}$$

where $c_{p,f}$ is the specific heat of species i ($\mathrm{H_2}$, $\mathrm{H_2O}$), h_f is the convective heat transfer coefficient between the solid (electrodes, electrolyte, bipolar plate combination) and the fuel, T_s is the solid temperature, and T_f is the temperature of the fuel gas.

Energy balance in the air channel:

$$z_a \frac{d\left(N\, c_{p,a}\, T\right)_a}{dx} = h_a \left(T_s - T_a\right) + c_{p,\mathrm{O_2}} n_{\mathrm{O_2}} T_a, \tag{11}$$

where $c_{p,a}$ is the specific heat of species i ($\mathrm{O_2}$, $\mathrm{N_2}$), h_a is the convective heat transfer coefficient between the solid (electrodes, electrolyte, bipolar plate combination) and the air, and T_a is the temperature of the oxidant gas.

Energy balance in the solid:

$$kt_m \left(\frac{d^2 T_s}{dx^2}\right) = \left(c_{p,\mathrm{H_2O}} n_{\mathrm{H_2O}} + h_f + h_a\right) Ts + \left(c_{p,\mathrm{O_2}} n_{\mathrm{O_2}} + h_a\right) T_a + \left(c_{p,\mathrm{H_2}} n_{\mathrm{H_2}} + h_f\right) T_f - q_s, \tag{12}$$

where k is the thermal conductivity of the composite material, t_m is the thickness of the composite material, and q_s is the heat generated in the electrolyte and is given by [12]

$$q_s = \frac{T_s\, \Delta S\, j}{2\,\mathcal{F}} + j\left(\eta_{\mathcal{O}} + \eta_{\mathcal{A}}\right), \tag{13}$$

where the first term indicates the heat liberated by the reaction and the second term indicates the heat generation by ohmic and activation polarizations.

2.3. Solution method

The system of equations described by Eq. (4) and Eqs. (9)-(12) constitute the entire set of equations needed to determine the local current density distribution, anode, cathode and solid temperature profiles, and gas distribution along the the fuel and oxidant channels. All the thermophysical properties were determined using the method of rational approximations [13]. The thermal conductivity of the solid component was determined by averaging the thermal conductivities of the individual components in relation to their masses [14]. The heat transfer coefficient was calculated by $h = \left(\mathrm{Nu}\, k_{\mathrm{Mix}}\right)/D_h$ (assuming a fully developed laminar flow in a channel with rectangular cross section), Nusselt number of Nu$= 3.39$ [15]) where D_h represents a characteristic diameter of the channels, and k_{Mix} is the thermal conductivity of the gas mixture (fuel or oxidant); the thermal conductivity of the gas mixture was calculated according to the Mason and Saxena modification to the Wassilijewa method [16].

The boundary conditions for the mass conservation equations are the initial molar flux rates, and for the energy balances the temperature at the inlet conditions in the fuel and oxidant channels. For the energy equation in the solid component, the two initial conditions are the inlet temperature and $d\,T_s/d\,x = 0$, assuming that the solid is insulated along the boundaries.

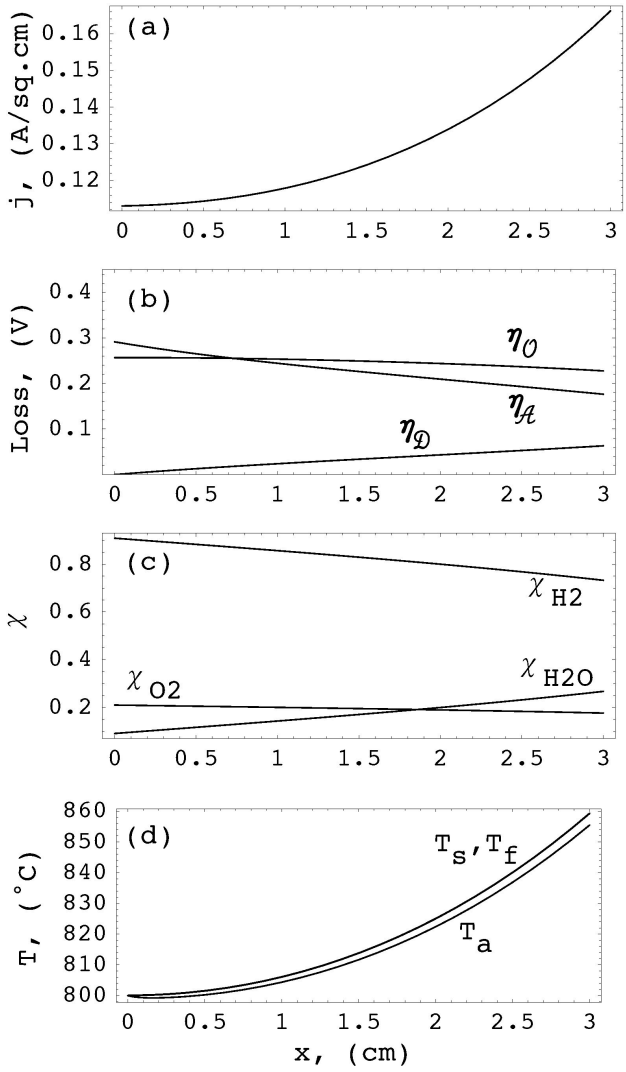

FIGURE 4. Electrolyte supported cell. (a) Local current density distribution, (b) Polarization distribution, (c) Concentration of hydrogen, water and oxygen, (d) temperature profiles. Initial temperature 1073 K, cell potential 0.50 volts.

The equations can be solved using any numerical technique for systems of differential equations (*e.g.*, finite differences or finite volume). However, for the sake of speediness we used Mathematica™.

3. Results and discussion

The operating conditions and design parameters are: cell potential of 0.5 volts, initial temperature of 1073 K (800°C), hydrogen flow rate 10.0×10^{-5} gm s^{-1} cm^{-2} (10% of water was added to the fuel stream), oxygen flow rate 80×10^{-5} gm s^{-1} cm^{-2} (air: $O_2/N_2 = 0.21/0.79$), channel height of 0.2 cm (air and fuel). A small square single cell is simulated with dimensions of 3 cm$\times$3 cm; thus the channel length is taken to be 3 cm. Two types of membranes were analyzed, *i.e.* electrolyte-supported and anode-supported. The electrolyte-supported cell has the following dimensions: electrolyte thickness of 500 μm, anode and cathode thickness of 50 μm, respectively. The anode-supported cell has the following dimensions: electrolyte thickness of 10 μm, anode thickness of 200 μm, and cathode thickness of 40 μm.

In Fig. 4, the results for an electrolyte-supported cell are shown. The main characteristic of this type of cell is the thick electrolyte, which serves as a support for the electrodes. The thick electrolyte increases the ionic resistance and therefore ohmic polarization becomes the limiting factor. In Fig. 4a, the local current density increases downstream as a result of a constant increase in temperature along the channel. As the temperature increases (see Fig. 4d) the ionic resistance decreases and ohmic polarization ($\eta_{\mathcal{O}}$) decreases as well (see Fig. 4b). However, because only a slight increase in temperature is observed, ohmic polarization decreases very slowly. Thus the increase in local current density is driven by a combination of a considerable decrease in activation polarization ($\eta_{\mathcal{A}}$) and a slight decrease in ohmic polarization; it was mentioned earlier than activation polarization decreases quickly as the temperature increases (see Fig. 4c-d). Diffusion polarization ($\eta_{\mathcal{D}}$) increased only at the end of the channel due to the reduction in the concentration of fuel. The fuel and oxidant concentrations (expressed as molar fractions, χ) are shown in Fig. 4d. Hydrogen and oxygen concentrations decrease because both are electrochemically consumed along the channel, while water is produced. The high concentration of hydrogen at the end of the channel indicates a low fuel utilization, which translates into the low values of current density. Accordingly, it is clear than a longer channel and higher temperature (*i.e.* lower ohmic polarization) could increase fuel utilization and reduce the total losses in the cell, and consequently increase the overall performance of the cell.

In Fig. 5, the results for an anode-supported cell are shown. The principal characteristic of anode-supported cells is the anode thickness, which is thicker by one order of magnitude than the thickness of the electrolyte or cathode. A reduction in the electrolyte thickness help to reduce the ionic resistance; therefore, the cell can be operated at lower temperatures. On the other hand, the increase in anode thickness augments the risk of diffusion limitations at the end of the channels because of the possibility of having fuel/oxidant starvation. Figure 5a shows the local current density along the channel. In this case, the values of the local current density were higher than for the case of an electrolyte-supported cell. The higher local current density is a result of an almost negligible ohmic polarization (see Fig. 5b), and a better fuel utilization, represented by a substancial decrease in the concentration of hydrogen (see Fig. 5c). The sudden drop in local current density at the end of the channel relates to the increase in diffusion polarization; as the fuel concentration reduces, diffusion polarization increases very quickly for relatively high values of current density (see Fig. 2b). Unfortunately, one disadvantage of anode-supported cells is the substantial increase in temperature (from 800 to 1100°C) see Fig. 5d. At this temperature, a slight mismatch in the

thermal expansion coefficient for the different components that make up the fuel cell could lead to fracture and consequently short circuit the cell. The state of the art SOFC materials comprise yttria-stabilized zirconia as electrolyte, niquel-yttria stabilized zirconia as anode, and strontium doped lanthanum manganite as cathode. These materials have been chosen, among other characteristics, because of their similar thermal expansion coefficients. However, the materials used to seal the cell (*e.g.* mica or glass-ceramic systems [17]) do not posses such characteristics, and at high temperatures the thermal expansion of these material will induce considerable thermal stress to the cell; thus a reduction in temperature is always a desired property for SOFCs.

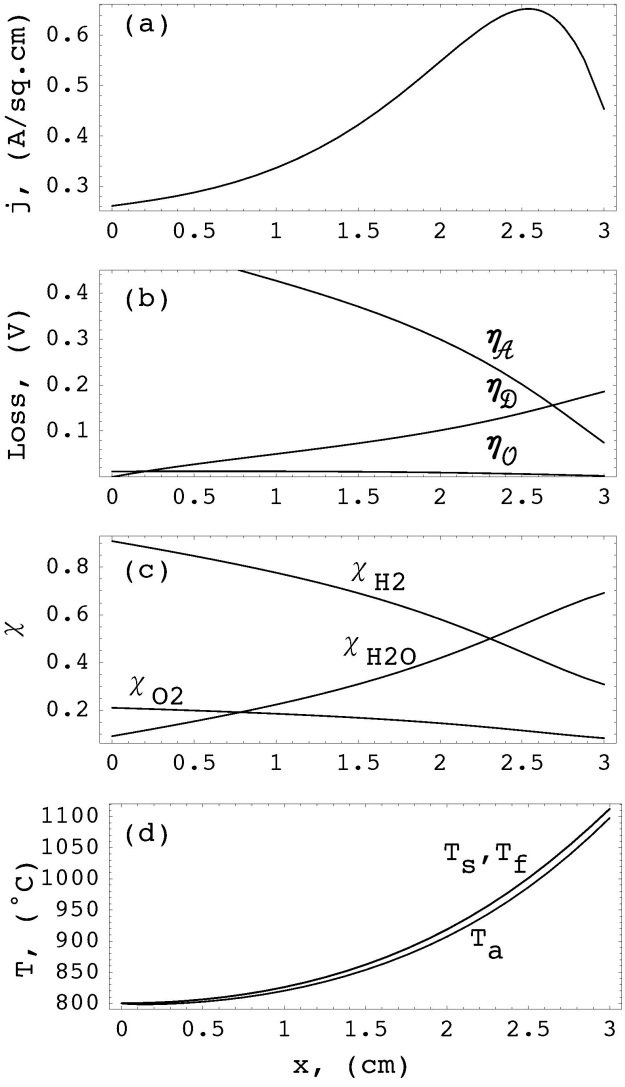

FIGURE 5. Anode supported cell. (a) Local current density distribution, (b) Polarization distribution, (c) Concentration of hydrogen, water and oxygen, (d) temperature profiles. Initial temperature 1073 K, cell potential 0.50 volts.

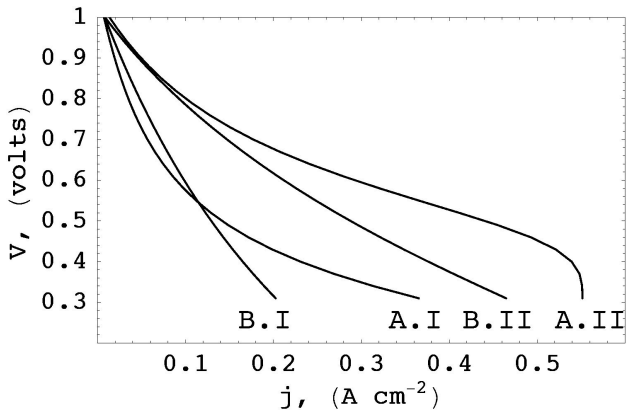

FIGURE 6. IV performance curves. A.I anode-supported cell at 700°C, A.II anode-supported cell at 800°C, B.I electrolyte-supported cell at 800°C, B.II electrolyte-supported cell at 900°C.

Finally, the performance characteristics of the cell (IV curves) are shown for an anode-supported cell and for an electrolyte-supported cell, see Fig. 6. The IV curves were created from the model by averaging the local current density at a fixed cell potential, and then the same process was repeated for the entire range of cell potential (*i.e.* from open circuit voltage to short circuit voltage). The results show that by increasing the temperature (from A.I: 700°C to A.II: 800°C for the anode-supported cell and from B.I: 800°C to B.II: 900°C for the electrolyte-supported cell, Fig. 6) the performance of the cell increases as well. At higher temperatures, activation and ohmic polarization decrease; thus higher potentials are expected. However, at high current densities, diffusion limitations from the anode-supported cell become apparent in the form of a quick drop in voltage (Fig. 6-A.II). The IV curves for the electrolyte-supported cell (Fig. 6-B.I and B.II) show a lower performance with respect to the anode-supported cell, even if the cell is operated at a higher temperature (Fig. 6-B.II vs. Fig. 6-A.II).

4. Final Remarks

A computer model was developed for determining the local current density distribution, the temperature profiles, and the gas concentrations along the channels that make up a single cell. In reality, single cells are piled into stacks to produce the desire power. Nevertheless, the model presented here can be extended, assuming a uniform flow rate of fuel and oxidant to all the channels in a single cell and in the stack. The model comprises a system of six differential equations (*i.e.* mass and energy conservation) and one algebraic equation (*i.e.* electrochemical potential). A solution to this system was implemented with Mathematica™.

The results showed that anode-supported cells gave a better performance in terms of higher local current densities and higher IV curves. The performance of an electrolyte-supported cell improved at higher temperatures, but still was lower than the anode-supported cell at a lower temperature.

Because high temperatures induce thermal stress in the cell, it is desirable to operate at low temperature. Accordingly, based on the results shown here, we believe that the optimal performance will be obtained by using an anode-supported cell at relative high cell potentials. Such conditions are attained to the left of the middle of the IV curve in Fig. 6-A.II (anode-supported case).

Acknowledgments

This material is based upon work supported by the National Science Foundation under grant No. 0093923. We also gratefully acknowledge the Mexican Federal Goverment, through the Secretary of Economy and CONACyT, and the State of Jalisco for their partial support of this project.

1. E. Services, *Fuel Cell Hndbook*, 6th ed. (Parsons, inc., Science Applicatrions International Corporation, 2002).
2. T.V. Nguyen and R.E. White, *Journal of the Electronchemical Society* **140** (1993) 2178.
3. N.Q. Minh and T. Takahashi, *Science and Technology of Ceramic Fuel Cells* (Elsevier, 1995).
4. E. Hernández-Pacheco, M.D. Mann, P. N. Hutton, D. Singh, and K.E. Martin, *International Journal of Hydrogen Energy* **30** (2005) 1221.
5. E. Hernández-Pacheco, D. Sing, P.N. Hutton, N. Patel, and M.D. Mann, *Journal of Power Cources* **138** (2004) 174.
6. P. Costamagna, A. Selimovic, M.D. Borghi, and G. Agnew, *Chemical Engineering Journal* **102** (2004) 61.
7. R. Suwanwarangkul *et al.*, *Journal Of Power Sources* **122** (2003) 9.
8. H. Zhu and R.J. Kee, *Journal of Power Sources* **117** (2003) 61.
9. P. Costamagna, P. Costa, and V. Antonucci, *Electrochemica Acta* **43** (1998) 375.
10. S.H. chan and Z.T. Xia, *Journal of the Electrochemical Society* **148** (2001) A388.
11. E. Achenbach, in *Modelling and Evaluation of advanced Solid Oxice Fuel Cells* (International Energy Agency Programme on R, D&D on Advanced fuel Cells, 1996).
12. M. Iwata *et al.*, *Solid State Ionics* **132** (2000) 297.
13. E. Hernández-Pacheco and M.D. Mann, *Journal of Power Sources* **128** (2004) 25.
14. J.R. Ferguson, in *International Sumposium on Solid Oxide Fuel Cells* (Comission of the European Communities, 1991) p. 305.
15. F.P. Incropera and D.P. DeWitt, *Fundamentals of Heat and Mass Transfer*, 5th ed. (John Wiley and Sons, LTD, 2002).
16. R.C. Reid, J.M. Prausnitz, and B.E. Poling, The Properties of Gases and Liquids, 4th ed. (McGraw Hill Book company, 1987).
17. P. Batfalsky, U. Diekmann, J.G. Maliszewski, and T.K. Julich, in *International Conference of Joining Ceramics, Grass and Metal*, edited by DVS-Berichte (1997), p. 72.